Use of Hydrometeors, Bragg Scatter, and Sun Spikes to Determine System Z_{DR} Biases in the WSR-88D Fleet

W. David Zittel

W. David Zittel[1], Jeffrey G. Cunningham[1], Robert R. Lee[1], Lindsey M. Richardson[1], Richard L. Ice[1], and Valery Melnikov[2]

[1]*NOAA, NWS, Radar Operations Center, 1200 Westheimer Dr, Norman, Oklahoma, USA*
[2]*National Severe Storms Laboratory, 120 David L. Boren Blvd, Norman, Oklahoma, USA*
18 July 2014

1. Introduction

Recently, the United States' National Weather Service completed an upgrade of its network of the Weather Surveillance Radar – 1988 Doppler (WSR-88D) to dual polarization. The new upgrade provides estimates of differential reflectivity (Z_{DR}), differential phase (PHI_{DP}), and correlation coefficient (RHO_{HV}). All three fields provide valuable information about the nature of hydrometeors and are used to identify the types of precipitation such as rain, hail, and / or snow in a hydrometeor classification algorithm (HCA). Where the HCA identifies light, moderate, or heavy rain (including rain with large drops), Z_{DR}, in combination with reflectivity (Z), is used by the WSR-88D's Quantitative Precipitation Estimate (QPE) Algorithm to estimate rain rate. While the WSR-88D requires a calibration of Z to within 1 dBZ, the required accuracy for Z_{DR} is 0.1 dB for the QPE algorithm to obtain optimal precipitation estimates.

To arrive at a true Z_{DR} value, the WSR-88D calculates and applies an offset to the measured Z_{DR} based on measured receiver, transmitter, and antenna path losses in the horizontal and vertical channels. Getting reliable hardware measurements for estimating Z_{DR} biases has proven challenging (Ice et al. 2013, Ice et al. 2014). As an alternate means of estimating system Z_{DR} bias, the authors have concentrated on evaluating external Z_{DR} measurements under conditions where the Z_{DR} estimate should inherently be near zero or can be adjusted to near zero. These conditions include two types of hydrometeors (light rain and dry snow), and clear-air returns from Bragg scatter for full path Z_{DR} bias estimates, and sun spikes for estimating receiver path biases only. These four conditions, being mutually exclusive, provide independent estimates for individual sites. This paper shows that biases from each full-path method, when averaged over several days, show similar results and can be used to determine trends.

2. Goal

A committee composed of meteorologists, radar engineers, and electronics technicians within the Radar Operations Center (ROC) and from the National Severe Storms Laboratory (NSSL) recently completed an internal study of the sources of system Z_{DR} bias fleetwide. They concluded that radar sites whose Z_{DR} bias exceeds ± 0.2 dB using the external methods "…should be flagged as having a potentially significant Z_{DR} bias." To address the sources of errors the team proposed changes / enhancements to the WSR-88D in four broad areas: 1) Radar Data Acquisition (RDA) Unit Test Software; 2) Radar Product Generator (RPG) Hosted Calibration Monitoring; 3) Dual Polarization Hardware Engineering (RF Pallet and Antenna Mounted Equipment); and 4) RDA Hosted External Target Z_{DR} Calibration. This paper presents external methods and prototype displays currently under development to address monitoring Z_{DR} system bias. Cunningham et al. (2013) demonstrated that the system Z_{DR} bias for about 60% of the WSR-88D fleet fell within ± 0.2 dB of 0 dB when using the light rain scanning method meaning that 40% were considered out of calibration. The goal of the ROC is to reduce the number of sites whose Z_{DR} bias exceeds ± 0.2 dB over the next few years. The methods and associated graphics in this paper are being transitioned into the WSR-88D's RPG and some methods may be moved to the RDA.

3. External Target and Sun Methods For Estimating Z_{DR} Bias

In this section the authors discuss three methods for obtaining the total system Z_{DR} bias. Two use hydrometeors, namely light rain and dry snow; the third method is from Bragg scatter in clear air. An additional

method, using the sun's signal seen at low elevation angles, provides a measure of the receive path bias. This technique, when combined with the other three, can provide a measure of the transmit path bias. Some early processing steps for each method are accomplished in the RPG and collected off-line into MATLAB software to generate long-term averages and fleet-wide statistics.

3.1. Light Rain PPI Scanning Method

3.1.1. Overview

One common way of determining Z_{DR} system bias is the so-called "bird bath" configuration. The radar is pointed vertically during periods of light rain and rotated through 360°. The measured Z_{DR} is averaged through 360° to remove direction-dependent responses. Therefore, biases that remain are mainly due to differences in the H and V channels. Any deviation from 0 dB in the measured Z_{DR} represents a bias (Gorgucci et al. 1999; Brandes 2000). This technique is most commonly applied to research radars. Unfortunately, the antenna mounted equipment (AME) for the dual polarization upgrade to the WSR-88D precludes the possibility of pointing the antenna vertically. Instead, the techniques described below collect information from Plan Position Indicator (PPI) scans at constant elevation angles above 1.0° up to 19.5°. Based on disdrometer studies at NSSL (Schuur et al. 2001; Schuur et al. 2005), Ryzhkov developed a table of reflectivity-based offsets to apply to Z_{DR} measurements. The following steps highlight the automated processing for the light rain method: 1) Collect Z_{DR} values from each radar volume scan during rain events from all radar sites; 2) Compute the Z_{DR} bias from light rain, correcting light rain Z_{DR} values by the empirically derived values; 3) classify each sample as stratiform or convective; 4) Divide the data samples up into three hour blocks; and 5) Collect the cases into WSR-88D network national maps and histograms.

3.1.2. Description

This method uses operational volume coverage patterns (VCPs) to estimate total system Z_{DR} bias from light rain (Cunningham et al. 2013). To minimize contamination from ground clutter, the method obtains data at elevation angles greater than 1° and ≥ 20 km from the radar. Two filters are applied to the reflectivity data: signal-to-noise ratio (SNR) > 20 dB and RHO_{HV} > 0.98 to ensure sure strong signal is processed in the light rain region. To eliminate contamination from frozen or partially melted hydrometeors from the melting layer, data (radar bins) must be at least 1 km below the bottom of the melting layer as determined by the WSR-88Ds Melting Layer Detection Algorithm (MLDA; Giangrande 2008). For each volume scan, reflectivity data are binned into six categories between 19.0 and 30.5 dBZ. The median value of all the Z_{DR} values in each category is computed as long as there are at least 200 radar bins per category. After computing the median Z_{DR} values for each reflectivity category, offsets based on empirically derived values from disdrometer data collected in Oklahoma, are subtracted. (The six offsets are 0.23, 0.27, 0.32, 0.38, 0.46, and 0.53 dB.) The adjusted Z_{DR} values are logged into the WSR-88D's Radar Product Generator System Status Log and retrieved off-line for further processing by MATLAB software. The total system Z_{DR} bias for each volume scan is computed by averaging the six empirically corrected categories together. Finally, a 12 volume running average of the Z_{DR} bias is applied to obtain a statistically reliable estimate for the light rain based method. Longer-term averages are computed during off-line processing discussed in Sections 4 and 5.

It is well understood that areas of weak reflectivity may be obtained near strong convective areas due to the presence of a few large drops. That is, a few large drops can have the same reflectivity as many small drops. The presence of large drops would bias the estimates of Z_{DR} high. Two other tests are applied to decrease the chance of big drop contamination due to the nearby presence of strong convection. Following a suggestion by J. Krause (2013, personal communication), the first test assumes that convection lofts many large drops above the melting level. At ranges above the melting level, if fewer than 40 radar bins have reflectivity values of 40 dBZ or more, the sample is classified as stratiform. The 40 bin threshold was determined from a one month empirical study which used data from all WSR-88D sites that had rain and valid Z_{DR} measurements. The second test, using data from the same study, focuses on data near the radar below the melting level. First, all radar bins which have SNR > 20 dB, RHO_{HV} > 0.98, and reflectivity values between 10 and 30 dBZ are tabulated. Then, using the same SNR and RHO_{HV} criteria, all radar bins with reflectivity values greater than 30 dBZ are tabulated. If 80% or more of the reflectivity

values were from the 10 and 30 dBZ reflectivity category, then the sample is classified as stratiform. If both tests classify a volume as stratiform the volume is designated as stratiform. However, both the stratiform-only precipitation system Z_{DR} biases and the estimates of Z_{DR} biases in the presence of strong convection are retained for further analysis.

A simple melting level technique (not the MLDA) is used in conjunction with these two tests. For the lowest elevation above 1.0°, the technique looks for RHO_{HV} values between 0.88 and 0.98 between ranges 37 km (20 nmi) and 167 km (90 nmi) from the radar. Data are restricted to reflectivity bins ≥ 25 dBZ. A 15-bin moving average is taken along each radial. If 12 or more of the 15 bins meet the filter criteria, the range is recorded. The melting level for each radial is set to the average range of the saved ranges. The melting level for the sample is computed as the average range of all the radials that meet the filter criteria. In order for a light rain estimate to be retained for inclusion in the fleet-wide estimates of system Z_{DR} biases based on light rain a site must have at least three contiguous hours of estimates.

3.1.3. Limitations

With the light rain scanning method described here the authors assume that Z_{DR} values of light rain can be adjusted to 0 dB for a large number of radar volumes (i.e., over a long duration) and that the convective/stratiform classification tests accurately separate the two precipitation modes. To date, there is little difference seen in statistics from stratiform-only rain and from statistics that include rain with convection. The authors also recognize that the disdrometer-based empirical corrections to Z_{DR} biases do not take into account variations due to seasonal and regional differences in drop size distributions, especially as regards warm-cloud maritime versus cold-cloud continental regimes and orographically enhanced precipitation. Some sites in the western United States will rarely obtain Z_{DR} bias estimates from rain due to the nature of the precipitation (doesn't meet 3-hour requirement) and the natural aridity of the climate.

3.2. Dry Aggregate Snow PPI Scanning Method

3.2.1. Overview

Although computations of Z_{DR} for regions identified as dry snow by the HCA have been routinely computed and saved in RPG's status log, only recently have the authors begun to examine their use as a measure of Z_{DR} bias. Melnikov (personal communication, 2014) suggested the measurements in regions classified as dry snow could be used to determine if Z_{DR} has a low bias. In the absence of mean canting, ice crystals, plates, and dendrites all would have a horizontal orientation relative to the ground and appear as only slightly canted relative to the radar beam at elevations between 0.5 and 19.5°. Such orientations should produce a positive Z_{DR}. Only aggregates would be expected to have a Z_{DR} near 0 dB. (Ice crystals oriented vertically due to an electrified field would yield a valid negative Z_{DR} bias but this should happen rarely.) Regions with dry snow consisting of aggregates, dendrites, and plates are expected just above the melting layer which would be expected to yield net positive Z_{DR} values. Straka et al. (2000), in a survey of literature on expected ranges of values for dual polarization parameters, suggests a range of 0.0 to 0.5 dB for Z_{DR} in dry aggregate snow for C band radars. The low Z_{DR} values assume the aggregates are small, low-density, nearly spherical, and may be tumbling. Thompson et al. (2014), in developing a winter hydrometeor classification algorithm, used Z_{DR} values for aggregates of near 0 dB for X, C, and S band radars. The authors have found that a downward adjustment of 0.2 dB for Z_{DR} estimates of dry snow yields results similar to the light rain and Bragg scatter methods.

3.2.2. Description

This method uses operational volume coverage patterns (VCPs) to estimate total system Z_{DR} bias from regions identified as dry snow by the HCA algorithm. To minimize contamination from ground clutter the method obtains data at all elevation angles greater than 1° that meet the height requirement and considers bins with reflectivity values between 15 dBZ and 25 dBZ respectively. Three filters are applied to the dry snow radar bins: signal-to-noise ratio (SNR) >= 20 dB; $0.98 < RHO_{HV} < 1.0$ to ensure sure strong signal is processed in the uniform dry snow region; and $PHI_{DP} < 100°$ to make sure the beam is not sampling heavy precipitation. To eliminate contamination

from liquid or partially melted hydrometeors from the melting layer, the data (radar bins) must be completely above the top of the melting layer but no more than 1 km above, as determined by the MLDA. If the air temperature at the ground is at or below freezing, a maximum height of one 1 km is used. For each volume scan, dry snow bins are considered if they meet the criteria discussed above. If the number of bins meeting the above criteria is at least 500 and the standard deviation of Z_{DR} in those bins is less than 0.5 dB, then the Z_{DR} values are averaged and 0.2 dB (the expected Z_{DR} of dry aggregate snow) is subtracted to get a delta Z_{DR} for the volume scan. The average delta Z_{DR} values for 12 running volume scans are averaged to obtain the estimated Z_{DR} bias. Operationally, these Z_{DR} values are logged into the WSR-88D's Radar Product Generator System Status Log and are retrieved off-line for further processing.

The rain Z_{DR} bias estimates are limited to times that rain is falling within the radar umbrella. Dry snow is observed in both summer and winter. Therefore, Z_{DR} bias estimates are available more frequently with the dry snow method than from the rain method.

3.2.3. Limitations

With the method described here, the authors assume that the Z_{DR} value for dry snow (aggregates, dendrites, and plates just above the melting layer) is ~0.2 dB and that the Z_{DR} values can be accurately corrected to 0 dB for a large number of radar volumes (i.e., over a long duration). Even though the dry snow method is not expected to accurately indicate high Z_{DR} biases, the method does show some correlation with the rain method for Z_{DR} bias values greater than 0 dB. However, the authors have great confidence that radars having Z_{DR} bias values less than -0.2 computed from dry snow are not well calibrated. If the MLDA estimate of the height of the melting layer is inaccurate, then our sampling method is in error. It is possible that as the radar beam passes through the melting layer, Z_{DR} estimates from the region above may be biased. The authors are conducting investigations into this possibility. In the winter, when the surface temperature is at or below freezing, this concern is eliminated.

3.3. Bragg Scatter PPI Scanning Method

3.3.1. Overview

Radar Height Indicator (RHI) type displays may be used to observe different types of radar returns. Fine scale, enhanced sampling in range and vertical resolution allows the discernment of discrete layers of clouds, biota, and Bragg scatter. Figure 1 from Melnikov et al. (2011) shows an example from the NSSL test bed radar KOUN in with a Bragg layer present. Bragg scatter results from density discontinuities in moisture and temperature, e.g. at the top of the convective boundary layer, due to turbulent eddies with a diameter ~one-half the size of the transmitted wavelength (i.e., ~5 cm for 10 cm WSR-88Ds). Melnikov et al. (2011) suggested that Bragg scatter, being isotropic, should have intrinsic Z_{DR} values of 0 dB. Cunningham et al. (2013) and Hoban et al. (2014) validated that the WSR-88D could indeed observe Bragg scatter during routine data collection.

Because Rayleigh returns from cloud drops or drizzle may be present within the same viewing area or even the same sampling bin as Bragg scatter, there is potential for a bias in the measured Z_{DR}. Knight and Miller (1998) suggested differences in equivalent reflectivity factor Z_e between S band (10 cm) and X (3 cm) band radars could be used to identify areas of pure Bragg scatter return, S band having much stronger return. The WSR-88D has only the S Band wavelength thus other approaches have been developed by the authors to isolate pure Bragg scatter. The approaches use statistical tests of weak reflectivity, in addition to filters based on signal-to-noise ratio (SNR), RHO_{HV}, and the base moments of velocity and spectrum width. The following steps highlight the procedures for finding Bragg Scatter: 1) Restrict data collection to VCPs 21 and 32 and elevations between 2.4 and 4.5 deg; 2) Omit data sets likely to be contaminated by Rayleigh scattering / precipitation; 3) Apply filters to base data moments, SNR, and RHO_{HV}, 4) Apply statistical filters to the distribution of Z_{DR} sampled over two-hour blocks and obtain a modal value; 5) Collect the values for assembling fleetwide national maps and histograms.

3.3.2. Description

Historically, sites are more likely to use VCPs 32 and 21 during periods of clear air than other VCPs (Cunningham et al. 2013). Thus, these are the only VCPs used for detecting Bragg scatter. (VCP 31 is a long-pulse

version of VCP 32 but is frequently used in winter precipitation events and so has been excluded.) A second test for light precipitation computes a frequency distribution of Z at ranges between 10 and 80 km and elevations between 2.4° and 4.5°. At the 90th percentile Z must be ≤ -3 dBZ. If this condition is satisfied, then further filters are applied. Values (radar bins) of Z_{DR} are retained if Z is < 10 dBZ, SNR is < 15 dB, SPW ≥ 0.5 m s^{-1}, absolute value of velocity (V) > 2.0 m s^{-1}, and RHO_{HV} is > 0.98 and < 1.05. Each volume scan must have at least 600 radar bins. After 12 volume scans (about 2 hours), or sooner if there are 10,000 radar bins of Z_{DR} accrued in the frequency distribution, a check for contamination by either biota or clutter is done by computing the interquartile range (IQR) of the Z_{DR} frequency distribution. The separation between the 25th and 75th percentile must be ≤ 0.9 dB. The modal value of the histogram provides a measure of Z_{DR} bias from Bragg scatter, assuming the criteria for this last test is satisfied. An example of Bragg scattering seen on the operational Raleigh, NC WSR-88D (KRAX) from May 25, 2013 for a one hour period between 15-16 UTC is shown in Figure 2. Histograms by radar site of the Bragg scattering are examined to determine the modal Z_{DR} value which are expected to be zero. For example, in Figure 2 the difference between zero and the histogram mode is -0.50 dB. Note the mode and the median have the same value indicating there is little skewness to the distribution and, thus, unlikely to be contaminated by biota or ground clutter. Currently, Bragg scatter estimates of system Z_{DR} bias for radars are computed offline – a time-consuming step. In the spring of 2015 with Software Build Release 16, estimates of Z_{DR} bias from Bragg scatter are scheduled to be available in the RPG System Status Log.

3.3.3. Limitations

From the previous section we see that Bragg scatter creates weak echoes. With weak echoes two important issues should be considered in measurements of the system Z_{DR}: 1) The system dynamic curve must be well measured; and 2) Possible noise influence should be eliminated. Issue one is illustrated in Figure 3 where the dynamic curve is depicted for the ROC testbed WSR-88D KREX as a function of SNR of input signal. The curve was obtained by injecting calibrated RF signals into the input of the polarization channels and measuring the Z_{DR} response with RDA's RVP8 processor. An ideal Z_{DR} response is represented by a horizontal line, i.e., the response does not depend on the power of input signals. There is a jump in Z_{DR} of about 0.12 dB from 20 to 30 dB SNR. For signal with SNR > 30 dB, a correction of 0.12 dB would have to be added. Such non-linearity could fall anywhere within the range of SNR values for a WSR-88D and would be especially important if that non-linearity fell at or below 15 dB, the SNR range for which we look for Bragg scatter. *The true system Z_{DR} dynamic curve should be measured for each WSR-88D.* Issue two is relevant to signal with SNR < 10 dB. At such signals, correct noise levels in the channels have to be known. System Z_{DR} is calculated from two measured powers in the channels P_H and P_V and two noise levels N_H and N_V as

$$Z_{DR} = 10 \log\left(\frac{P_H - N_H}{P_V - N_V}\right) (dB) \quad (1)$$

It is seen that at weak signals, N_H and N_V should be known with sufficient accuracy. The noise powers are measured in the WSR-88D in radial-by-radial basis (Build 14, fielded spring 2014). For such measurements, the noise impact in Z_{DR} calculations is corrected.

Additionally, some contaminants, particularly biota and drizzle, may pass through the filters and skew Z_{DR} bias estimates to more positive values. These contaminants may or may not fall within the same range bin as Bragg but do contribute if they fall anywhere between 10-80 km in the allotted time window. The authors concede that a few valid (uncontaminated) Bragg cases are excluded with the rigorous filters, but the sensitivity to contamination necessitates stringency.

3.4. Sun Spikes

High resolution scanning of the sun at λ = 11 cm (Lang 1977) indicates no detectable linear polarization but there may be limited circular polarization due to sunspots. Holleman et al. (2010) demonstrated that one could track the Z_{DR} receive path bias from the sun on two European 5 cm radars. Cunningham et al. (2013) demonstrated use of the sun spikes to measure the receive path bias for the 10 cm WSR-88Ds. In particular, they calculated where the sun spike should occur morning and evenings near the 1.5° elevation angle for VCP 32 or the 1.5° and

2.5° elevation angles for VCP 31. (For these VCPs and elevation angles the azimuthal resolution is 0.5°.) To avoid clutter contamination they ignored the first 20 km. Finally, they required there be at least 1000 range bins (0.25 km resolution) with an SNR between 10 and 15 dB.

Beginning in the spring 2014 (Software Build 14) the WSR-88D began using a radial-by-radial noise estimation algorithm in the RDA (Ivić et al. 2013). This algorithm effectively removes the visual sun spike because it looks like noise. Figure 4 shows a notch in the direction of the evening sun spike for the Frederick, Oklahoma WSR-88D (KFDR). In lieu of searching for a sun spike, the authors examine the base data for the estimated noise in dB for the H and V channels ensuring that there is a peak in noise estimation in both the H and V channels in the same radial. Figure 5 shows a plot of the H and V noise estimation for the same time as in Figure 4. Note there is a peak of > 10 dB about 275° azimuth. Time indicated on the chart is the start of the elevation scan. However, the radial number within in the scan is number 112 out of 720 and the time to complete the scan is 72 sec so the scan time needs to be adjusted by ~11 sec. Using the adjusted time, the NOAA Solar Position Calculator indicates the sun's position is at 274.79° azimuth and 1.23° solar elevation for KFDR for a nominal difference of 0.21° in azimuth and 0.27° in elevation. The receiver Z_{DR} bias is $Z_{DR} = N_H - N_V\ (dB)$ or ~-0.03 dB. This analysis is done during off-line processing.

4. Shade Charts

Shade charts, a convenient way to show trends in data with time graphically, are generated for light rain, snow, and Bragg scatter methods for system Z_{DR} bias. For each method, median values are obtained for one-week discrete periods over several months. Where the bias is negative the shading is blue; where the bias is positive the shading is red. Shading is quantized to the native resolution of the Z_{DR} data or 0.0625 dB. The beginning point for shading is centered on the one-week interval. Two consecutive weekly medians must be obtained in order to create a shaded area. Where the shaded area is horizontal to the abscissa, the medians have the same value. Where the median shaded areas have slope, the median value for the second week has changed. Where there is no shading, the bias may be 0 dB or there simply may be no estimates available. If there is only one value for a week, the median is the nearest quantization level; for two values the median is considered the closest quantization level to the average of the two values. For three or more points, the median of the values is rounded to the nearest quantization value.

Figures 6a-c and 7a-c show examples of shade charts from two representative WSR-88Ds: Boston, Massachusetts (KBOX) and Tulsa, Oklahoma (KINX). In Figures 6a and 7a, a stratiform estimate is plotted as a plus sign (+) while a convective event is plotted as a small bullet (·). Both stratiform and convective estimates are considered when creating a shade chart for the light rain method. The dry aggregate snow method (Figs 6b and 7b) plots an asterisk ($*$) for each individual estimate. The Bragg scatter method (Figs 6c and 7c) plots individual estimates as a multiplication sign (×). Both the light rain and snow methods require at least 3 hours of contiguous data from which to estimate a system Z_{DR} bias. If the event exceeds 6 hours, the time period is split between the first 6 hours and the additional time considered separately. Up to four estimates per day are possible but the coverage is not required to fall within a 24 hour window. Gaps within a 6 hour window are allowed as long as they do not exceed 6 hours. For Bragg scatter, only the time between 17 and 19 UTC is currently examined. This allows, at most, one estimate per day per site based on the mode of the histogram (Section 2.3.2.), when Bragg scatter is detected. The time period chosen favors the eastern and central time zones where the authors initially looked for Bragg scatter. With the Build 16 Software Release (Spring 2015), data fleetwide will be examined continuously for Bragg scatter. This will provide estimates from the mountain and western time zones at times better suited to localized maximum heating.

Initial inspection of Figures 6a-c and 7a-c shows that the system Z_{DR} bias estimates for KBOX are all negative (shaded blue) while the estimates for KINX are all biased high (shaded red). Further inspection shows that, of the three methods for estimating system Z_{DR} bias, the light rain method has the fewest number of weeks with shading while the snow method has a much larger number of weeks with shading. Bragg scatter for these two sites provides almost as great a frequency of weekly estimates as the snow method. (Sites with no bias would, of course, have no shading.) Both charts show that the variance of individual estimates of Z_{DR} bias is largest for the snow method and smallest for the Bragg scatter method. For KBOX (Fig 6) a trend to a greater negative bias (~0.15 dB to ~0.30 dB) appears around the first week of November, 2013 reflected in both the snow and Bragg scatter methods. The light rain estimates of system Z_{DR} bias seen after the middle of November support the biases seen

by the other two methods. KINX shows good agreement in the estimate of the system Z_{DR} bias of ~0.20 dB between the light rain and the Bragg scatter methods. The snow method shows a somewhat smaller bias of ~0.10 dB. While these two sites show generally good agreement between the three methods, not all sites are as well-behaved. Work is ongoing to understand the differences. The next section discusses the availability of estimates for each method by time of year and geographical location.

5. Fleetwide Statistics

Recently, the ROC upgraded its capacity to store Level 2 data from all of the WSR-88Ds in the fleet to a full year. (Previously, the limit was about 3 months.) This upgrade provides the ROC the ability to determine seasonal and regional climatologies for each observational method for estimating system Z_{DR} bias as well as determine long-term trends in Z_{DR} bias for individual sites. As the ROC refines the methods, they can be tested and validated on longer data sets.

5.1. Geographical / Seasonal Availability of the System Z_{DR} Bias Estimates

A median Z_{DR} from all events observed during a month is tabulated for each WSR-88D site and for each of the three methods. Figures 8a-d and 9a-d show the system Z_{DR} bias estimates for January and May 2014. Figures 8a and 9a show the geographical distribution and estimated Z_{DR} bias for the light rain method from events identified as stratiform, Figures 8b and 9b show the geographical distribution of the combined stratiform and convective events for light rain, Figures 8c and 9c show the geographical distribution and estimated Z_{DR} bias for snow events, and Figures 8d and 9d show the geographical distribution and estimated Z_{DR} bias for the Bragg scatter method. Green shaded boxes show sites whose monthly estimated bias is within ± 0 .2 dB, blue shaded boxes show sites whose monthly estimated bias is < -0.2 dB, and red shaded boxes show sites whose monthly estimated bias is > 0.2 dB. Gray shaded boxes indicate no estimate was available. Currently, the only requirement is there be a least one event in a month to provide an estimate.

In January (Fig 8a), with one exception, only the Atlantic and Gulf Coasts of the United States (US) have estimates from stratiform rain events. If we add the convective events the coverage expands diagonally westward for the eastern third of the country. By contrast, nearly all of the contiguous states have an estimate of Z_{DR} system bias from snow (Fig 8c). Estimates of Z_{DR} system bias from Bragg scatter for January were available for nearly all the country (Fig 8d). As the west coast has a Mediterranean type climate or a modified Mediterranean climate one would have expected more estimates of from light rain. The authors speculate that the west coast experienced unusually dry conditions this past winter and, when precipitation did occur, the freezing level was too low to provide estimates from light rain. It is also somewhat surprising to see a large number of western sites reporting Bragg scatter. Normally, density discontinuities due to moisture gradients are assumed to provide the largest contribution to Bragg scatter echo and surface air in January should be dry in clear air. However, recent in-house work suggests wind shear can also provide Bragg scatter-like radar echo. The authors also recognize that the 17-19 UTC time window is not optimal for daytime heating to generate turbulent mixing at the top of the convective boundary layer in the western half of the country.

For May (Fig 9a), the geographical distribution of Z_{DR} system bias estimates from light stratiform rain has expanded to fill much of the eastern half of the US but the western half of the country is still almost entirely lacking in observations. If one adds the convective events (Fig 9b) to the light rain distribution, the central plains states now have Z_{DR} bias estimates. By contrast, all sites have an estimate of the system Z_{DR} bias from the dry snow method (Fig 9c). The geographical distribution of estimates for the Bragg scatter method for May (Fig 9d) shows coverage through most of the US with notable areas in the south central US (Texas and Oklahoma) and the northeast US (Pennsylvania and New York) lacking observations. Here, the radar sites may not be using the two VCPs (32 and 21) we use to look for Bragg scatter and there also may be contamination from biota (most likely insects) during the limited 2-hour window. The distribution for June (not shown) shows an expanded area in the central US without Bragg scatter estimates due, presumably, to even more biota being present.

The authors expect that when the initial estimates for Bragg scatter become available 24/7 in the RPG, the coverage will expand. With refinement of pertinent filters, the method may be able to include more VCPs.

5.2. Numerical Distribution of System Z_{DR} Biases

To assess the fleet-wide Z_{DR} performance, the estimates of system Z_{DR} biases for each event (as shown in the shade charts) are tabulated monthly for the light rain method (with and without the convective cases), the snow method, and the Bragg scatter method. Figures 10a-d and 11a-d show the frequency distribution for each method for January and May 2014, respectively. The light stratiform rain method, with only 57 total events, indicates 57% of the events are within ± 0.2 dB of 0 dB while 32% are < -0.2 dB and 11% are > 0.2 dB. When one includes the January convective events, the total number of events jumps to 279 but the percent of events that are within ± 0.2 dB changes nominally to 60%. The percent < -0.2 dB is 24% and the percent > 0.2 dB is 16%. In May the number of events with stratiform rain only jumps to 183 and 58% lie within ± 0.2 dB of 0 dB. The percent of these events with estimated system Z_{DR} biases < -0.2 dB is 25% while the percent of events > 0.2 dB is 17%. These percentages align closely with the light rain method with the combined stratiform and convective events. That is, there is a noticeable skewness to negative biases. However, when one combines both the convective and stratiform light rain events, the May distribution shows that 28% of the events have a bias > 0.2 dB while only 16% have a bias < -0.2 dB. The percent of events (56%) is within ± 0.2 dB of 0 dB and is consistent with the other light rain distributions. One explanation for the shift in the distribution is that the reflectivity-based corrections to the mean Z_{DR} overcompensates in winter and stratiform events but undercompensates for the combined stratiform and convective events in light rain in warmer months. An interesting exercise would be to examine the distribution of the convective-only light rain events. There may be more contamination from large drops than we realize.

The snow method has a total of 2058 events in January with 62% within ± 0.2 dB of 0 dB. The percent that are less than -0.2 dB is 24% while the percent above 0.2 dB is 14%. May has a total event count of 3791 with 60% of the events within ± 0.2 dB of 0 dB. The percent of events < -0.2 dB is 26% and the percent of events > 0.2 dB is 14%. The snow method, with a greater number of events for both January and May, has a more nearly Gaussian distribution than the frequency distributions for light rain. While the percent of positive and negative outliers are close, there a small shift in the peak modal value which is near 0 dB for January but ~-0.1 dB in May. Possibly the 0.2 dB downward adjustment, while appropriate for winter, may be overcompensating in the summer.

Figures 12a and 12b show the distribution of the monthly median estimated system Z_{DR} biases from Bragg scatter for January and May, respectively. In January 72% of the events lie within ± 0.2 dB of 0 dB and in May 77% of the events are within this range. The estimated system Z_{DR} biases that exceed ± 0.2 dB in January are balanced at 14% on each side. In May 9% of the biases are below -0.2 dB and 14% > 0.2 dB. The Bragg scatter method shows fewer sites that are greater than 0.2 dB from 0 dB than either the light rain or snow method for estimating system Z_{DR} bias. The authors believe the Bragg scatter method is superior to the precipitation-based methods because it does not rely on empirical correction terms. However, the reason for there being fewer sites with a Z_{DR} bias exceeding ± 0.2 dB from 0 dB than the other methods is a continuing area of study.

The Bragg scatter estimate, as currently computed, is limited to one estimate from 17-19 UTC daily and when a radar site is using either VCP 21 or 32. The number of sites reporting one or more events in January was 113 and the equivalent number for May was 110. A comparison of Figures 12a and 12b show that there were considerably more events in January than in May (841 compared to 328). The disparity in number of events is due to the greater likelihood of a site using VCP 32 in winter than in summer; despite the drier air, Bragg scatter was detected. Also, during the winter months there are fewer insects, a common source of contamination in the Bragg scatter. Finally, some filters were developed on data from winter months and may need retuning for warm season months.

6. Comparison of Receiver / Transmitter Biases Between Internal and External Calibration Methods

Ice et al. (2014) provides a comprehensive description of the calibration methods done within the WSR-88D to determine antenna, receiver, and transmitter biases from which to develop a Z_{DR} offset that is applied to the Z_{DR} data field. In general this can be formulated as

$$Z_{DR}(offset) = (SMB + RCB) + (SMB + TXB) = 2 * (SMB) + RCB + TXB \quad (2)$$

where SMB is the sun measurement (antenna) bias, RCB is the receiver bias, and TXB is the transmitter bias as calculated internally in the RDA. Following Cunningham et al. (2013) the intrinsic Z_{DR} values for sun spikes should be 0 dB unless there is a receiver or antenna bias or

$$Z_{DR}(measured) = Z_{DR}\,(intrinsic) + RCB + SMB \tag{3}$$

or simply

$$Z_{DR}(measured) = RCB + SMB. \tag{4}$$

where $Z_{DR}(measured)$ is the values computed in the RDA. In practice, the RDA applies the $Z_{DR}(offset)$ to $Z_{DR}(measured)$ so both the transmit and receive path bias corrections are automatically applied to Level 2 data sent downstream to the RPG. Because the transmit path bias plays no role in the sun spike measurements, the $Z_{DR}(offset)$ may artificially bias the Level 2 sun spike data. Therefore, we remove it as follows:

$$Z_{DR}(level2) = Z_{DR}(measured) - Z_{DR}(offset) \tag{5}$$

Rearranging terms yields

$$Z_{DR}(measured) = Z_{DR}(level2) + Z_{DR}(offset). \tag{6}$$

For the sun there is no weather signal so the $Z_{DR}(measured)$ is simply

$$Z_{DR}(measured) = RCB + SMB = Z_{DR}(sun). \tag{7}$$

Rearranging terms from Eq. 2 yields the engineering transmit path bias estimate as

$$TXB + SMB = Z_{DR}(offset) - (RCB + SMB) \tag{8}$$

The engineering transmit path bias ($TXB + SMB$) may be compared to observationally-derived transmit path biases by subtracting the sun spike receive path bias from any of the full-path bias estimators $Z_{DR}(rain)$, $Z_{DR}(snow)$, *or* $Z_{DR}(Bragg)$:

$$Z_{DR}(txb) + SMB = Z_{DR}([rain: snow: Bragg]) + Z_{DR}(offset) - Z_{DR}(sun) \tag{9}$$

where $Z_{DR}(txb) + SMB$ is the transmit path bias estimated by removing the sun-estimated receive path bias from the full-path bias based on external targets; the offset, previously removed, must be added back in.

Besides the $Z_{DR}(offset)$, most of the internal hardware measurements are reported routinely in the base data stream (Level 2 data) or are static. This allows us to compute the engineering-derived receive and transmit path biases with which to compare to externally-derived receive and transmit path biases. Figure 13a shows a comparison between the engineering receive path bias to the observationally-derived receive path bias. Figure 13b shows a comparison between the engineering transmit path bias and the observationally-derived external transmit path bias. Note that while the sun-based receive path bias has a < 0.1 dB difference from the internally computed receive path bias, the internally computed transmit path bias is different from the computed methods based on dry snow and light rain by ~0.3-0.5 dB. The net bias is ~0.2 dB too high as seen in the shade charts for this site. From these charts one can conclude there is a hardware calibration issue in the transmit path.

7. Conclusions

This paper shows three different methods for estimating full-path system Z_{DR} biases that are obtained under mutually exclusive meteorological conditions. The dry snow method assumes the HCA accurately identifies types of precipitation and both the light rain and snow methods assume the MLDA accurately reports the height of the

melting layer. The Bragg scatter method provides good estimates when there are no sources of contamination either from cloud droplets / drizzle, biota, or ground clutter. Each method has geographical and seasonal limitations, but the dry snow method provides estimates from more sites than the other full-path methods. It is available regardless of season but does require precipitation above the melting layer. Both the light rain and dry snow methods have high variability over short periods of time (< 1 day) even when considering a three-hour average. Bragg scatter has potential to provide bias estimates with lower variability with proper filtering. Estimates from all three methods can provide consistent results (± 0.2 dB) when they are temporally close (within a week or two.) All methods require finding a central value over a week to remove variability and to show long-term trends in system Z_{DR} bias. The receive path Z_{DR} bias can be estimated by examining sun spikes or radial noise estimates from the radial-by-radial noise estimation algorithm. Measurements from external targets / sources may be used to provide an independent comparison to estimates of system Z_{DR} bias from the WSR-88D dual polarization hardware components.

Acknowledgments

The authors thank their colleagues within the ROC and in NSSL for their stimulating discussions regarding the development of this work and especially the reviewers for suggesting improvements to this paper.

References

Brandes, E., 2000: Dual polarization radar fundamentals and algorithm prospects, System Technology Associates, Contract Number 50RANW500051, 49 pp. [Available online at http://www.roc.noaa.gov/wsr88d/PublicDocs/AppsDocs/algorithm00.pdf.]

Cunningham, J. G., W. D. Zittel, R. R. Lee and R. L. Ice, 2013, Methods for identifying systematic differential reflectivity (Z_{DR}) biases on the operational WSR-88D network, *36th Conference on Radar Meteorology.* [Available at http://ams.confex.com/ams/36Radar/webprogram/Manuscript/Paper228792/JCunningham_36thRadarConf_9B5.pdf.]

Giangrande, S. E., J. M. Krause, and A. V. Ryzhkov, 2008: Automatic designation of the melting layer with a polarimetric prototype of the WSR-88D radar. *J. Appl. Meteor. Climatol.,* 47, 1354–1364.

Gorgucci, E., G. Scarchilli, and V. Chandrasekar, 1999: A procedure to calibrate multi parameter weather radar using properties of the rain medium. *IEEE Trans. Geosci. Remote Sens.* , **37**, 269- 276.

Hoban, N. P., J. G. Cunningham, and W. D. Zittel, 2014: Estimating systematic WSR-88D differential reflectivity (Z_{DR}) biases using Bragg scattering. *30th Conf. on Environmental Information Processing Technologies*. Atlanta, GA. Amer. Meteor. Soc. [Available online at http://ams.confex.com/ams/94Annual/webprogram/Manuscript/Paper237404/Final_Extend_Abstract_AMS_Feb2014.pdf.]

Ice, R. L., A. K. Heck and J. G. Cunningham, 2013: Polarimetric weather radar calibration – engineering challenges, *36th Conference on Radar Meteorology,* Breckenridge, CO. Amer. Meteor. Soc. [Available online at http://ams.confex.com/ams/36Radar/webprogram/Paper228789.html.]

Ice, R. L., A. K. Heck, J. G. Cunningham and W. D. Zittel, 2014: Challenges of polarimetric weather radar calibration, *8th European Conference on Radar and Hydrometeorology,* Garmisch-Partenkirchen, Germany.

Ivić, I. R., C. Curtis, and S. M. Torres, 2013: Radial-based noise power estimation for weather radars. *J. Atmos. Oceanic Technol.* **30**, 2737-2753.
doi: 10.1175/JTECH-D-13-00008.1.

Knight, C. A., and L. J. Miller, 1998: Early radar echoes from small, warm cumulus: Bragg and hydrometeor scatterings. *J. Atmos. Sci.,* **55**, 2974-2992.

Lang, Kenneth R., 1977: High resolution polarimetry of the sun at 3.7 and 11.1 cm wavelengths. *Solar Physics,* **52**, 63-68.

Melnikov, V., R. J. Doviak, D. S. Zrnić, and D. J. Stensrud, 2011: Mapping Bragg scattering with a polarimetric WSR-88D. *J. Atmos. Oceanic Technol.*, **28,** 1273-1285.

Schuur, T. J., A. V. Ryzhkov, and D. S. Zrnić, 2001: A statistical analysis of 2D-video-disdrometer data: impact on polarimetric rainfall estimation. Preprints, *30th International Conference on Radar Meteorology,* Munich, Germany. Amer. Meteor. Soc.

Schuur, T. J., A. V. Ryzhkov, and D. R. Clabo, 2005: Climatological analysis of DSDs in Oklahoma as revealed by 2D-video disdrometer and polarimetric WSR-88D radar. Preprints, *32nd Conference on Radar Meteorology,* Albuquerque, NM. Amer. Meteor. Soc.

Straka, J. M., D. S. Zrnić, and A. V. Ryzhkov, 2000: Bulk hydrometeor classification and quantification using polarimetric radar data: synthesis of relations. *J. Appl. Meteor.*, **39**, 1341-1372.

Thompson, E. J., S. A. Rutledge, B. Dolan, V. Chandrasekar, and B. L. Cheong, 2014: A dual-polarization radar hydrometeor classification algorithm for winter precipitation. *J. Atmos. Oceanic Technol.,* **31**, 1457-1481. doi: 10.1175/JTECH-D-13-00119.1

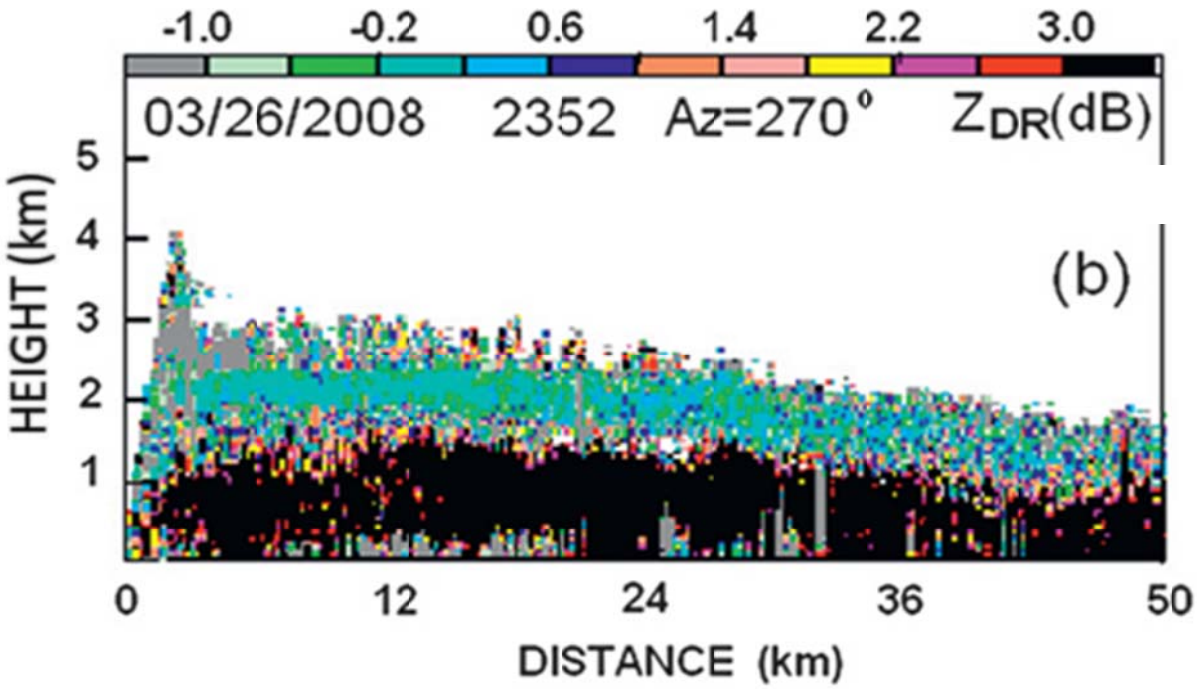

Figure 1. Vertical cross section of Z_{DR} (dB) above Norman, OK at 0000 UTC 21 Feb. 2008 (Melnikov et al. 2011). The predominantly blue and green layer about 2 km is from Bragg scatter; the black layer below 1.5 km shows echo from biota, most likely insects.

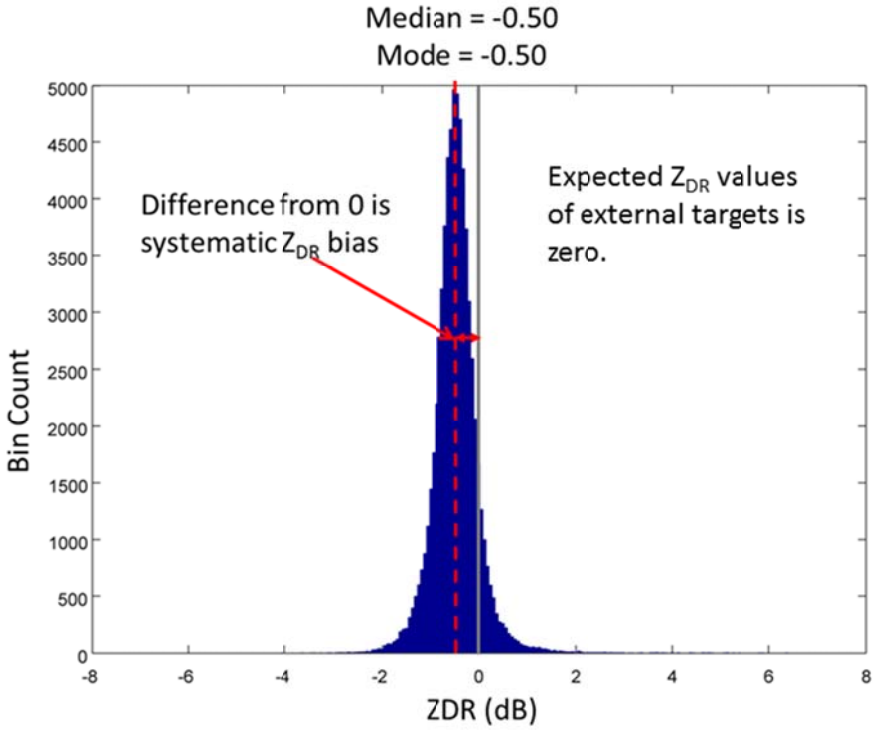

Figure 2: Histogram of Z_{DR} values from radar bins identified as containing Bragg Scatter from KRAX on May 25, 2013 for 15-16 UTC.

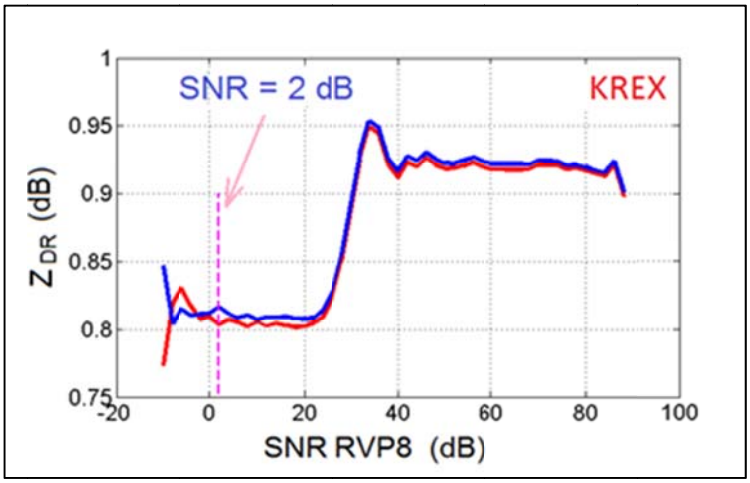

Figure 3. Z_{DR} system response for the ROC test-bed WSR-88D KREX. The SNR from a calibrated RF signal generator is shown in the abscissa. The vertical dashed line is for SNR = 2 dB; the radar variables are measured in the WSR-88Ds at signals with SNR >= 2 dB.

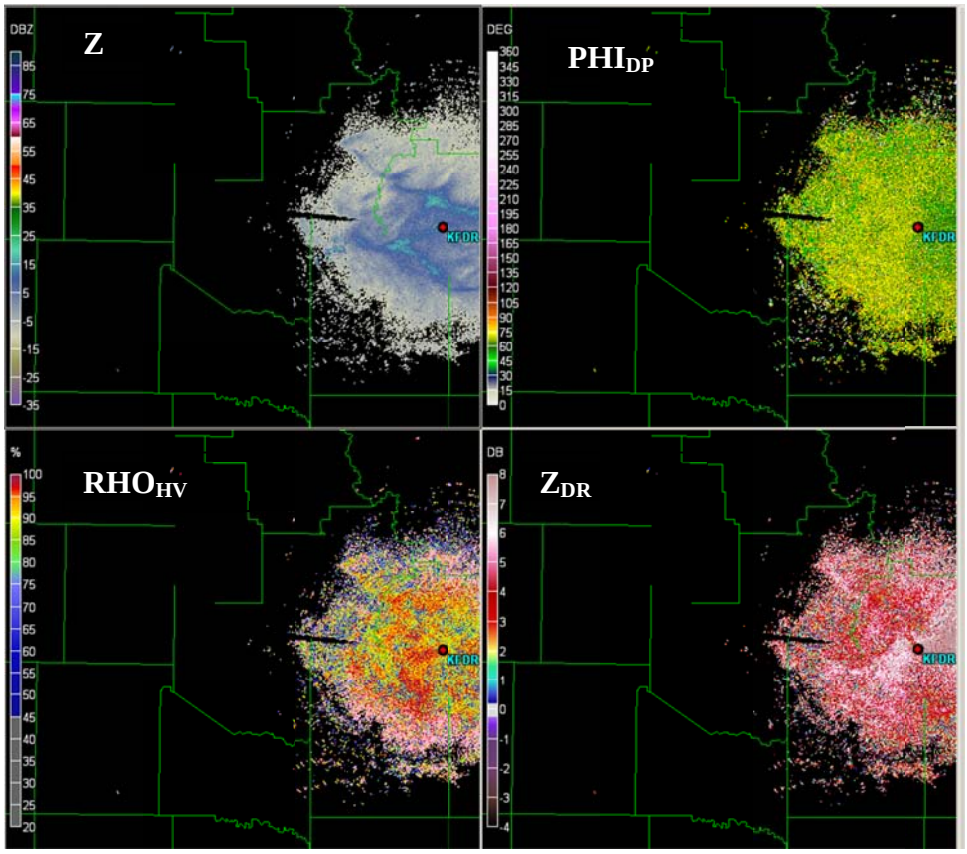

Figure 4. Example of sun spike removed by the radial-by-radial noise estimation algorithm around the 275° azimuth from the KFDR WSR-88D. Instead of a sun spike there is a notch in the remaining signal due to the elevated noise floor. The elevation is 1.5° and the VCP 32.

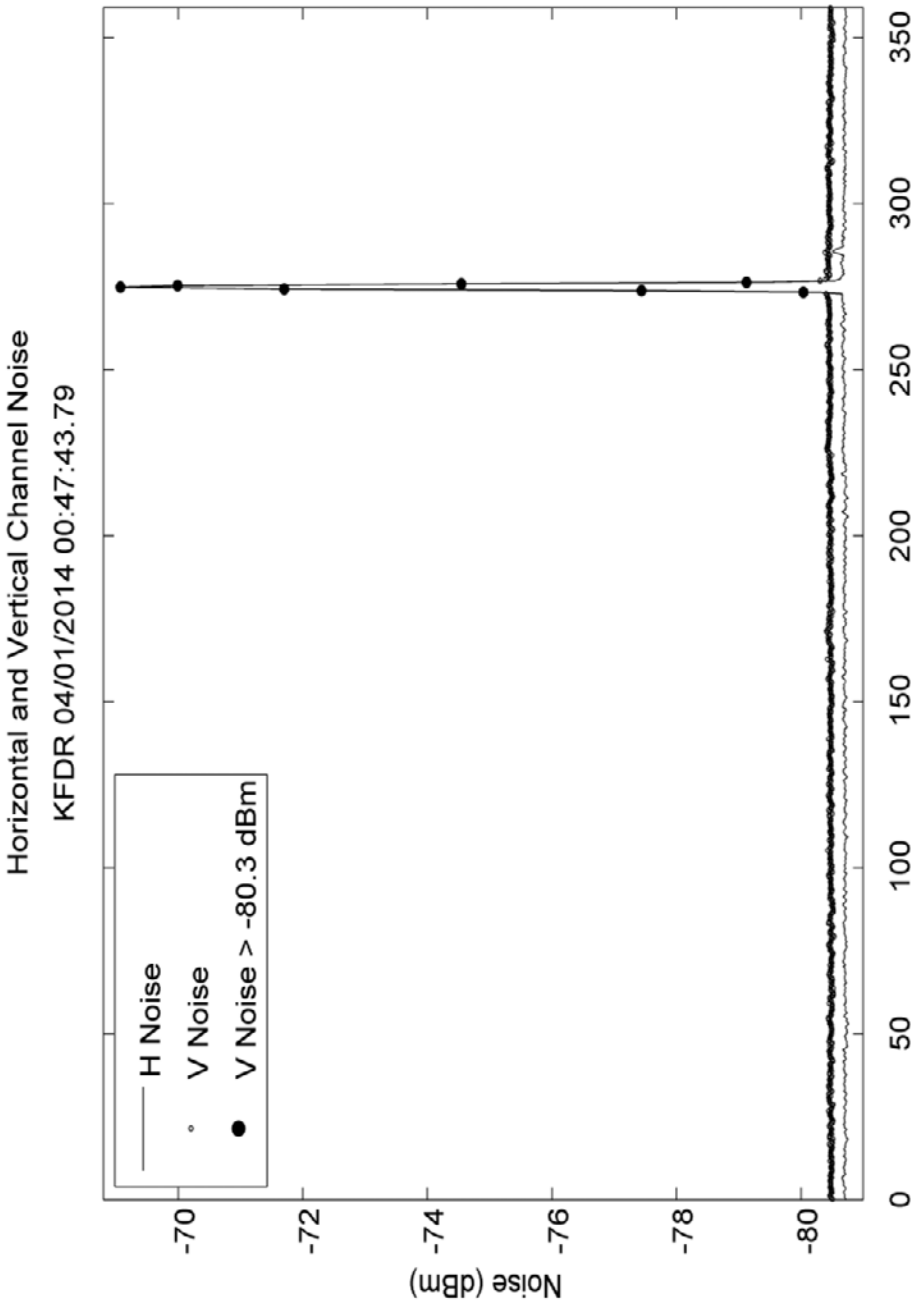

Figure 5. Estimates by radial of noise in H and V channels for the same radar as in Figure 4. The jump in noise around 275° azimuth is due to the interference from the sun detected by the radial-by-radial noise estimation algorithm. The difference in the peaks ($H_N - V_N$) is -0.03 dB.

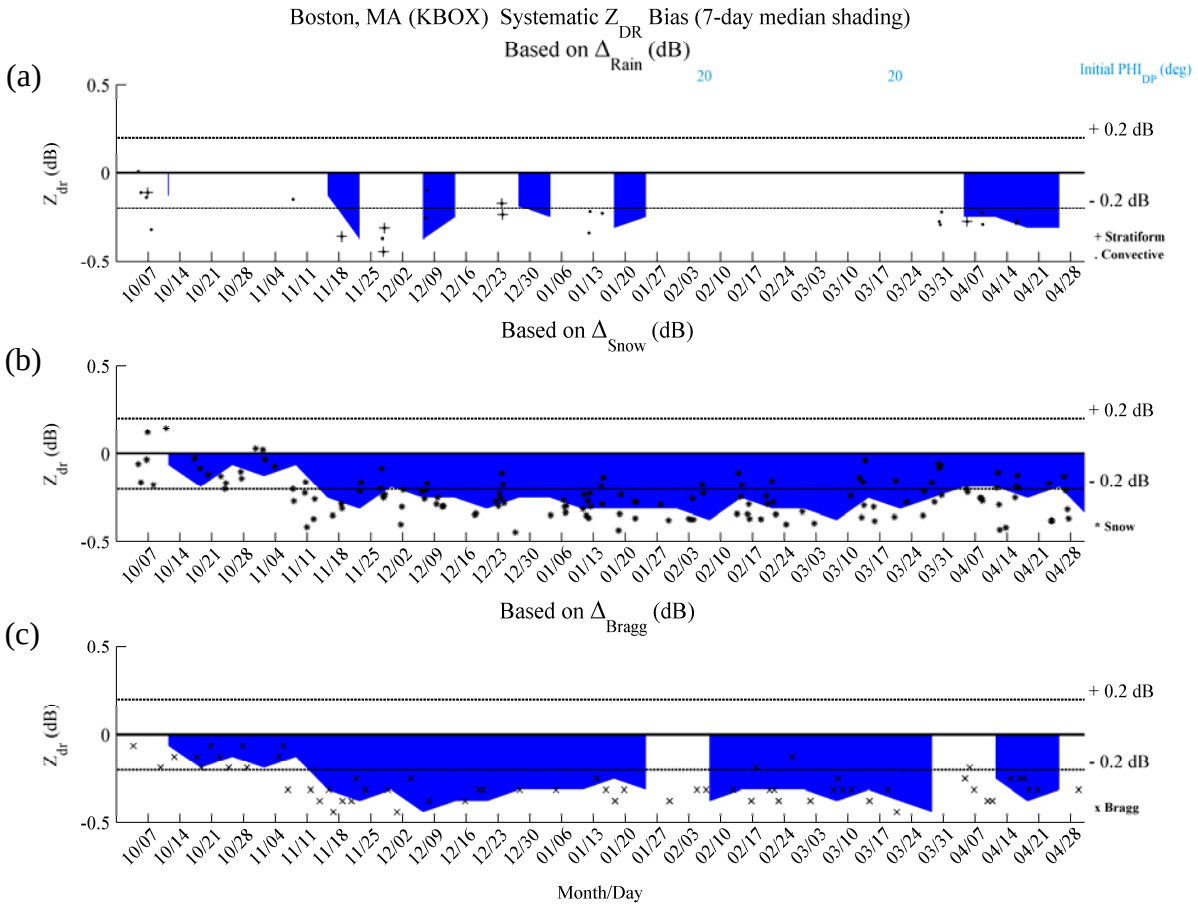

Figure 6: Z_{DR} shade charts for Boston, Massachusetts (KBOX) WSR-88D. Top panel (a) shows the trend and bias for the light rain method, the middle panel (b) shows the trend and bias for the dry snow method and the bottom panel (c) shows the trend and bias for the Bragg scatter method. The time period is from 1 Oct 2013 through 30 April 2014. Blue shading denotes negative bias. Note the agreement in the size of the bias between the three methods. ± 0.2 dB are shown as horizontal lines above and below the 0 dB line.

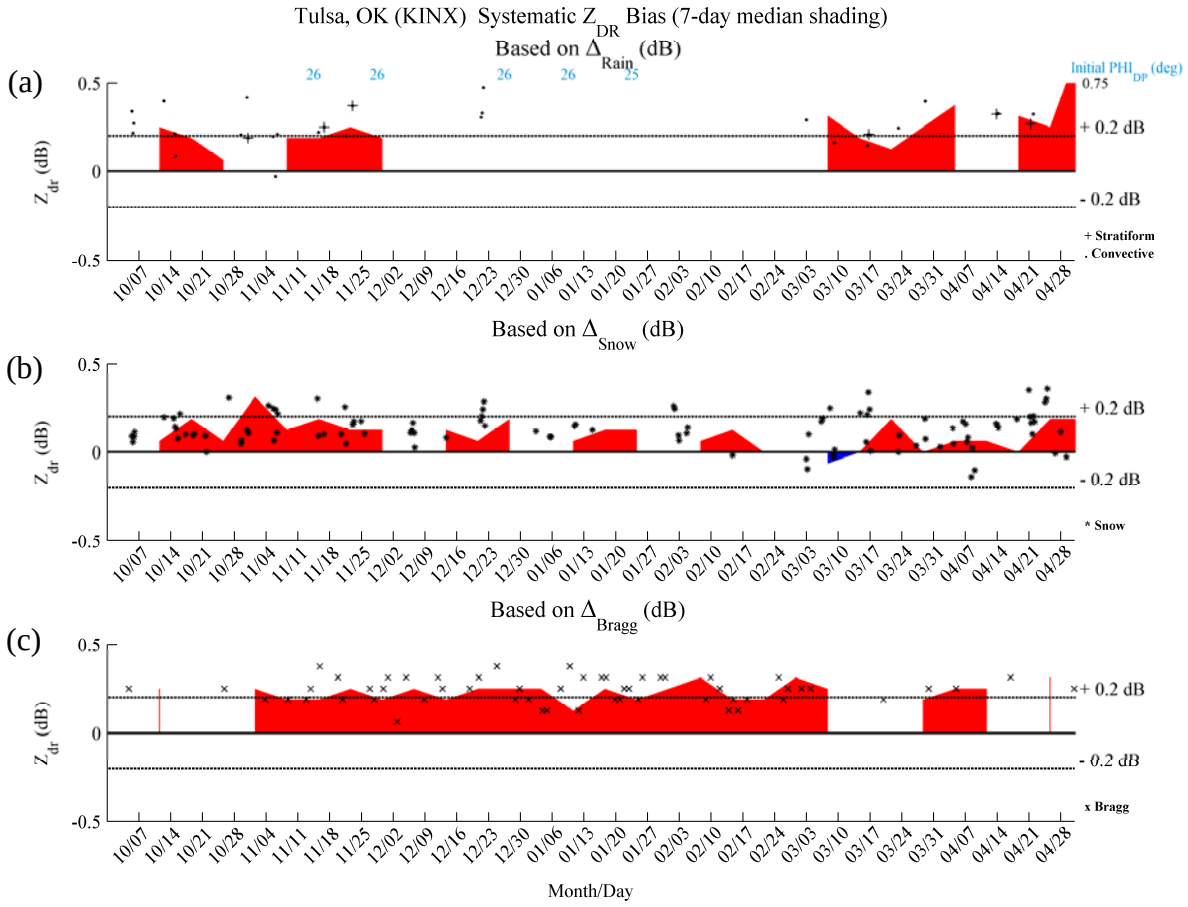

Figure 7: Z_{DR} shade charts for Tulsa, Oklahoma (KINX) WSR-88D. Top panel (a) shows the trend and bias for the light rain method, the middle panel (b) shows the trend and bias for the dry snow method and the bottom panel (c) shows the trend and bias for the Bragg scatter method. The time period is from 1 Oct 2013 through 30 April 2014. Red shading denotes positive bias. While the Bragg and light rain method are in general agreement, the snow method appears slightly smaller on average. ± 0.2 dB are shown as horizontal lines above and below the 0 dB line.

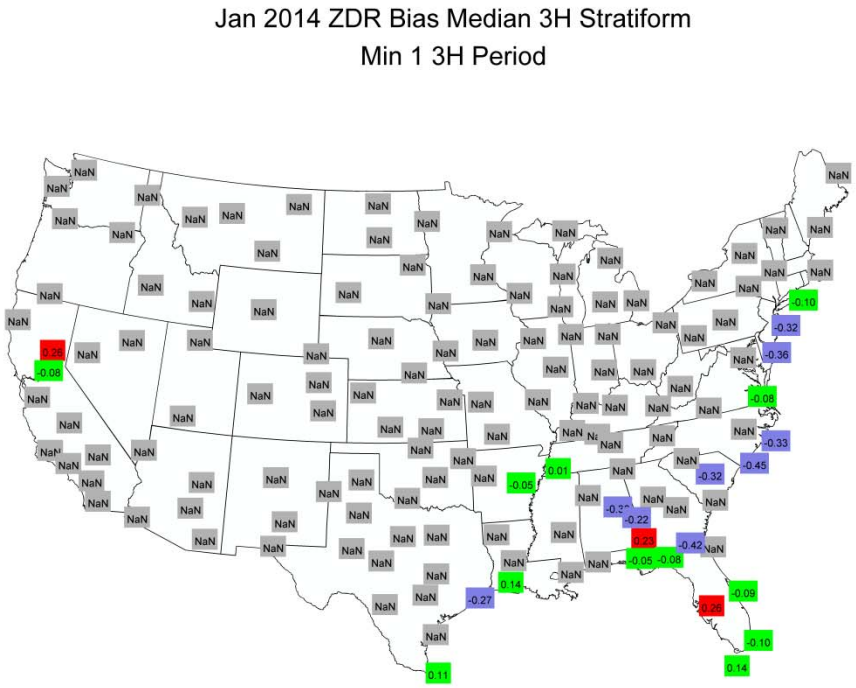

Figure 8a. Geographical location of WSR-88D sites with estimates of system Z_{DR} bias from stratiform rain for January 2014 for the contiguous lower 48 states. Green boxes show bias estimates within ± 0.2 dB; red boxes show sites with bias estimates > 0.2 dB; blue boxes show sites with bias estimates < -0.2 dB. Within each box is the estimated system Z_{DR} bias for a radar site. Gray boxes show sites for which no bias was available.

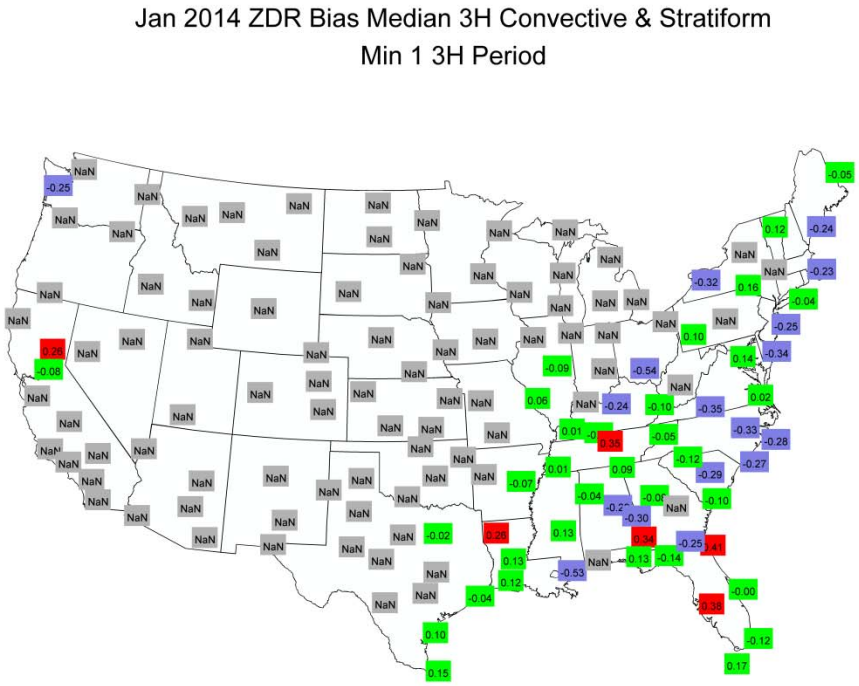

Figure 8b. Same as Figure 8a but based on stratiform and convective rain events for estimating system Z_{DR} bias.

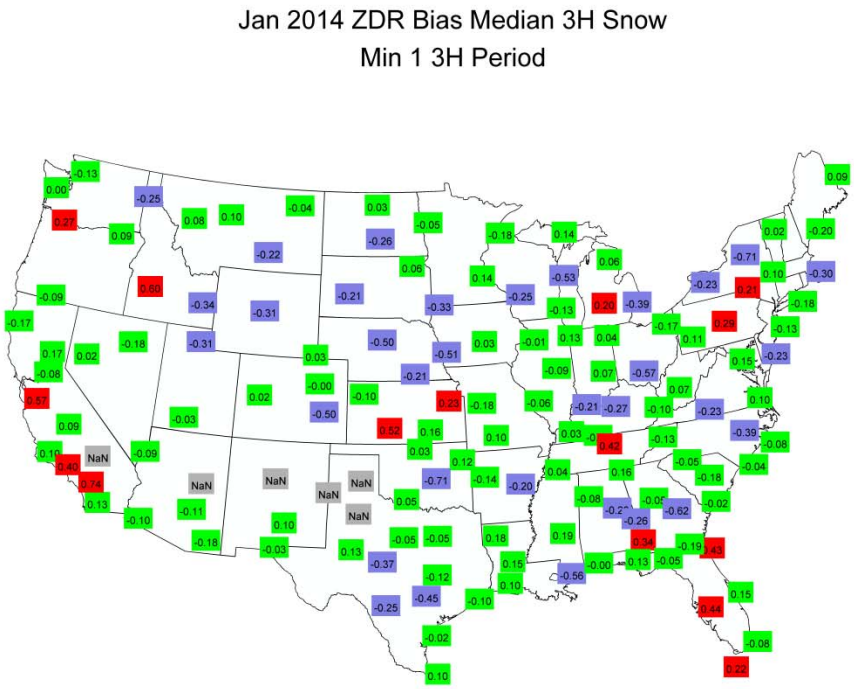

Figure 8c. Same as Figure 8a but based on the snow method for estimating system Z_{DR} bias.

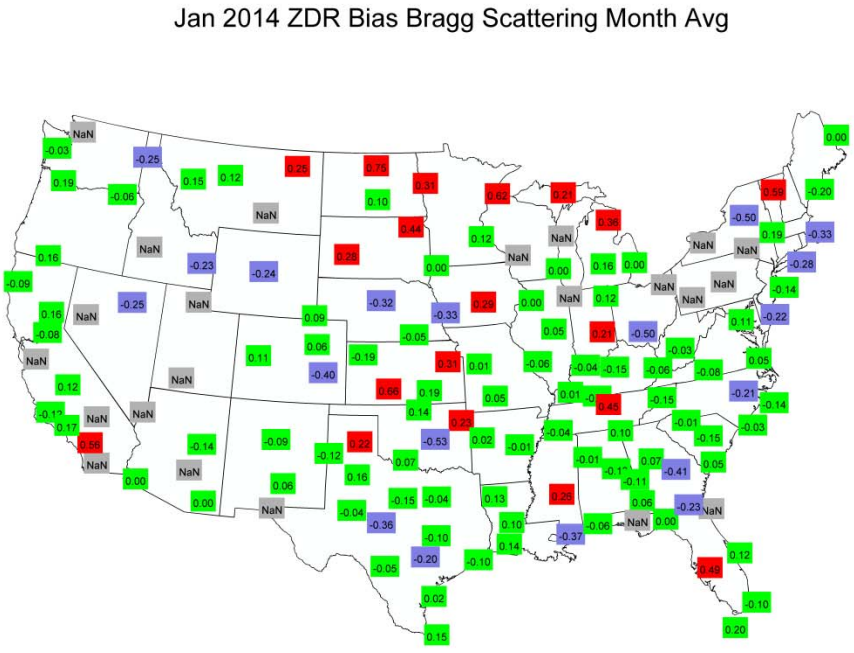

Figure 8d. Same as Figure 8a but based on the Bragg method for estimating system Z_{DR} bias.

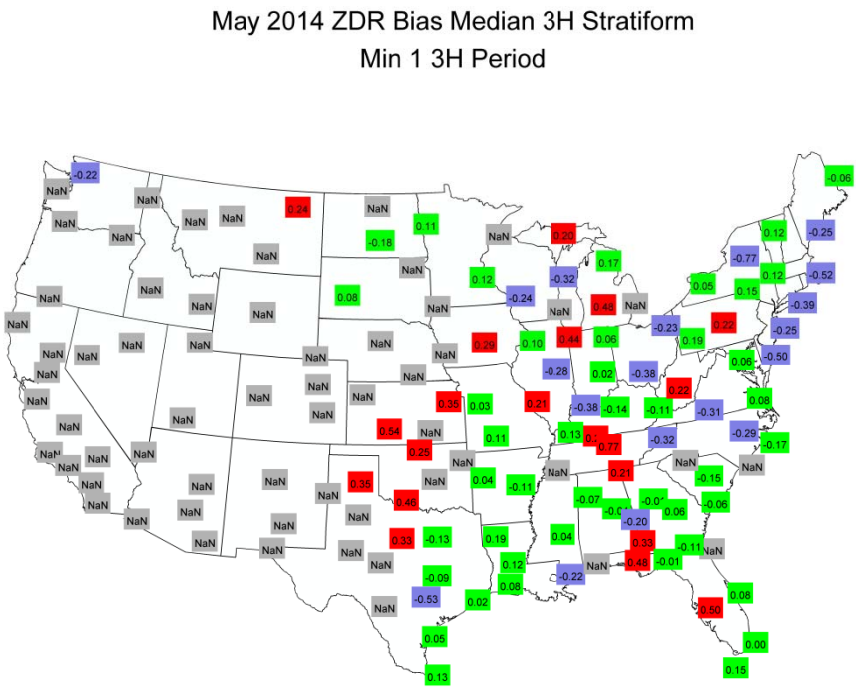

Figure 9a. Geographical location of WSR-88D sites with estimates of system Z_{DR} bias from stratiform rain for May 2014 for the contiguous lower 48 states. Green boxes show bias estimates within ± 0.2 dB; red boxes show sites with bias estimates > 0.2 dB; blue boxes show sites with bias estimates < -0.2 dB. Within each box is the estimated system Z_{DR} bias for a radar site. Gray boxes show sites for which no bias was available.

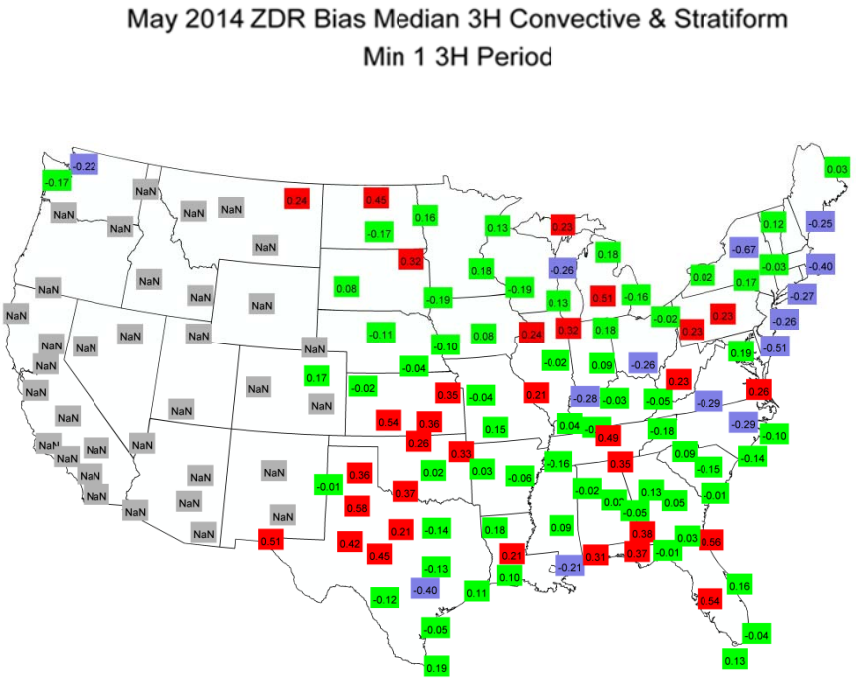

Figure 9b. Same as Figure 9a but based on stratiform and convective rain events for estimating system Z_{DR} bias.

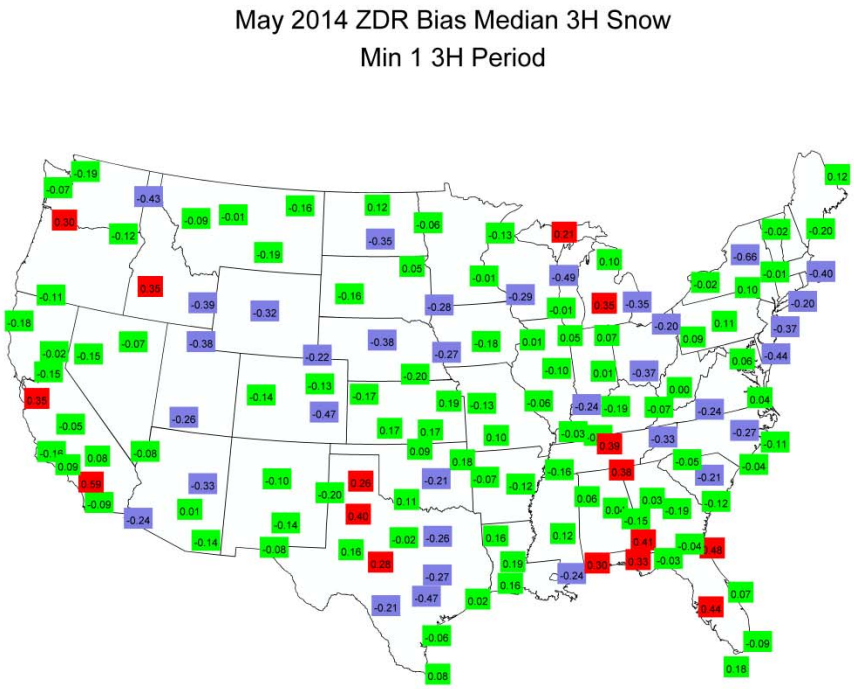

Figure 9c. Same as Figure 9a but based on the snow method for estimating system Z_{DR} bias.

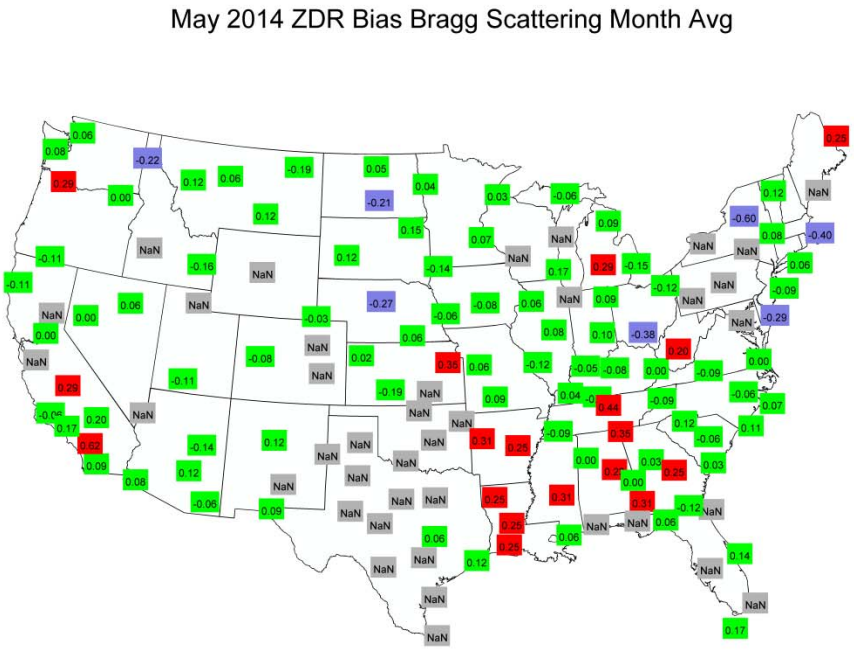

Figure 9d. Same as Figure 9a but based on the Bragg method for estimating system Z_{DR} bias.

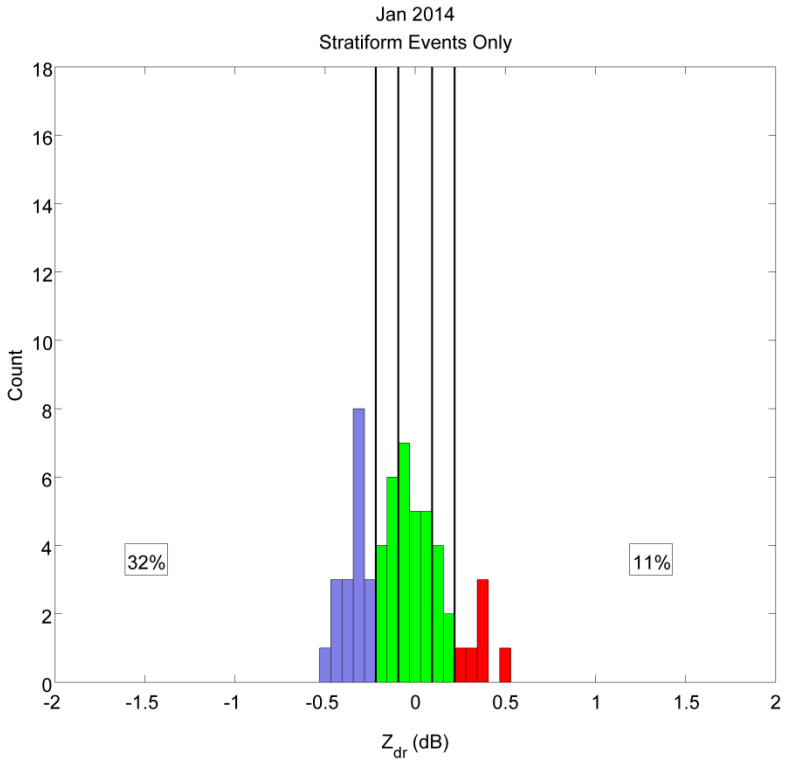

Figure 10a. Frequency distribution of median system Z_{DR} biases for January 2014 for the light rain method for stratiform events only.

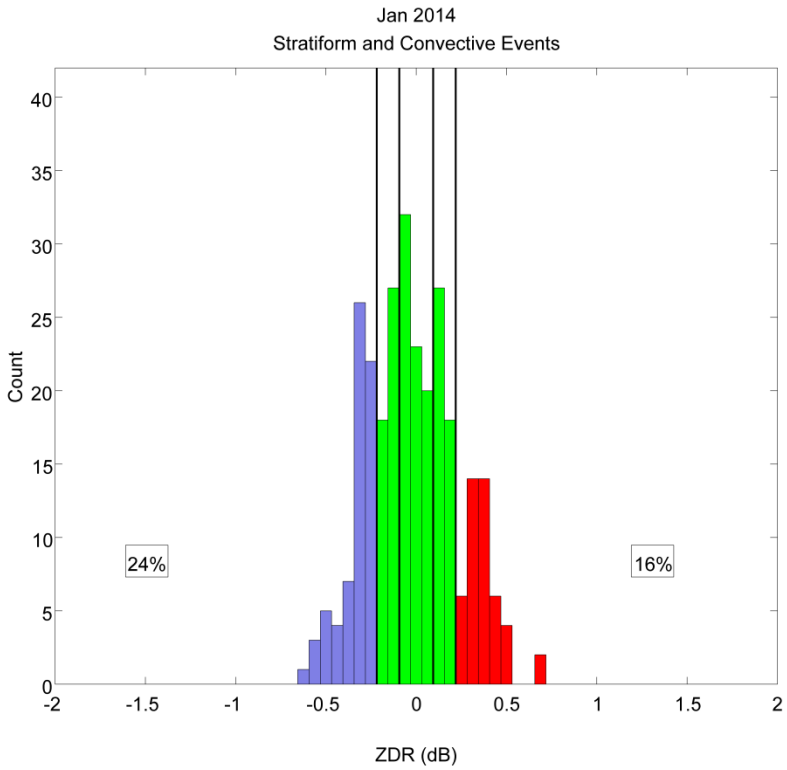

Figure 10b. Same as Figure 10a for the light rain method but with stratiform and convective events combined.

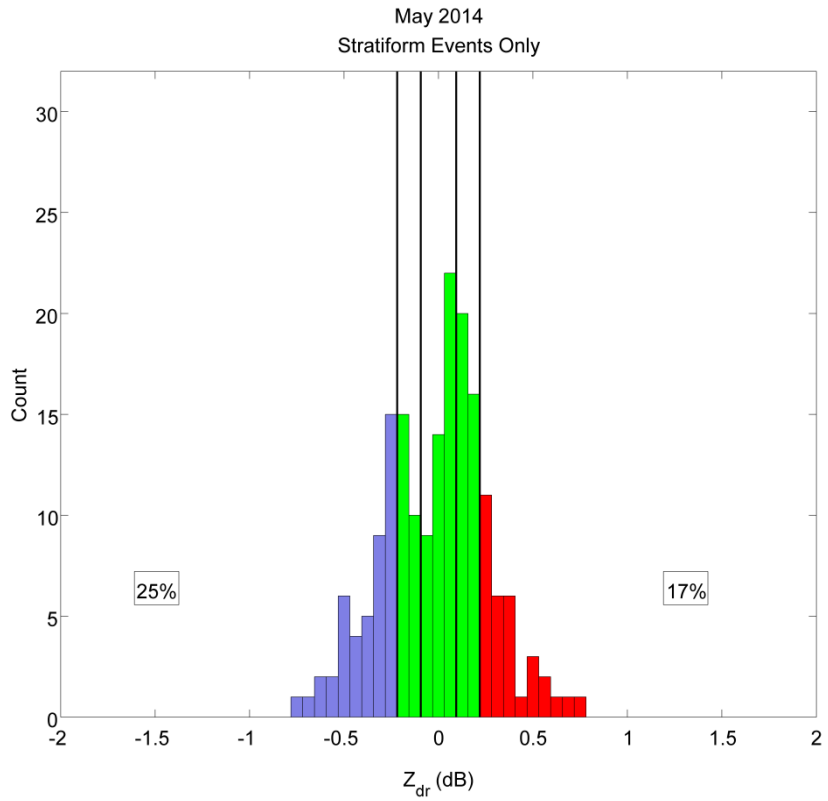

Figure 10c. Same as Figure 10a but for May 2014 for the light rain method with stratiform events only.

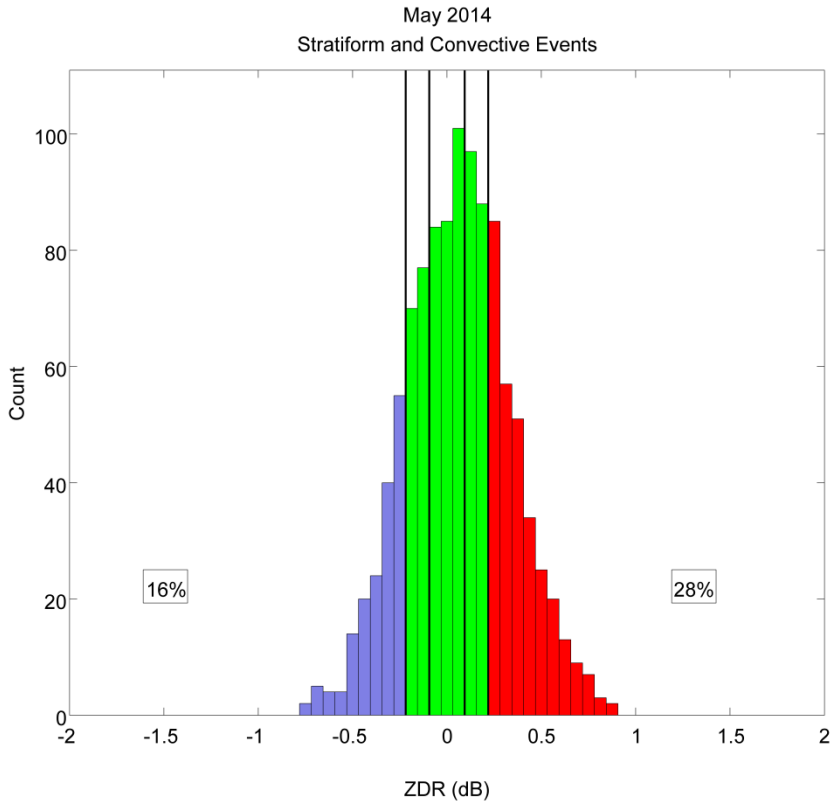

Figure 10d. Same as Figure 10c but with stratiform and convective events combined.

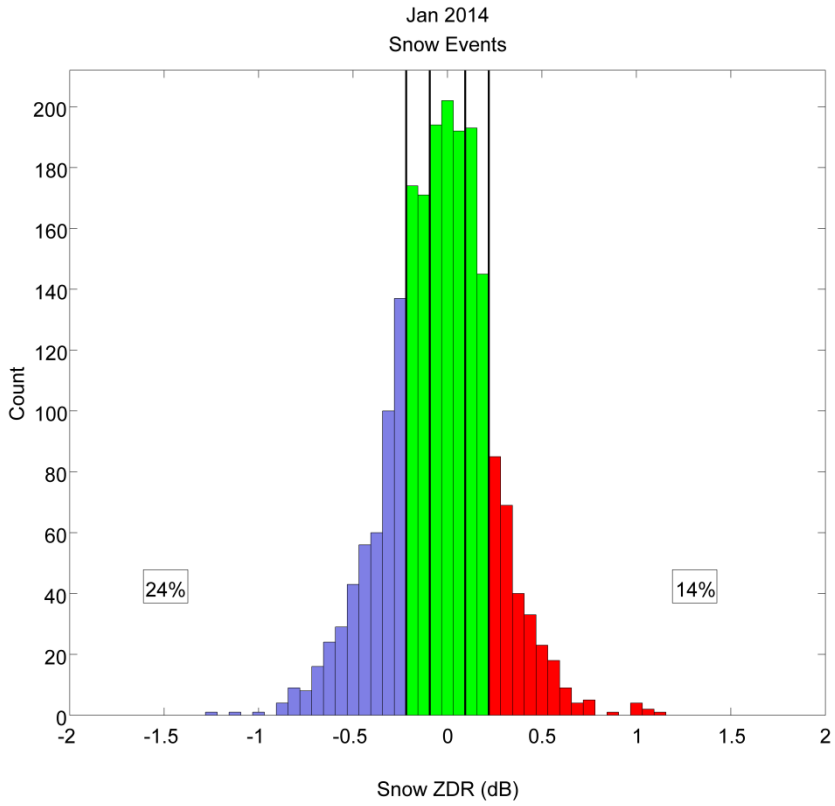

Figure 11a. Frequency distribution of median system Z_{DR} biases for the snow method for January 2014.

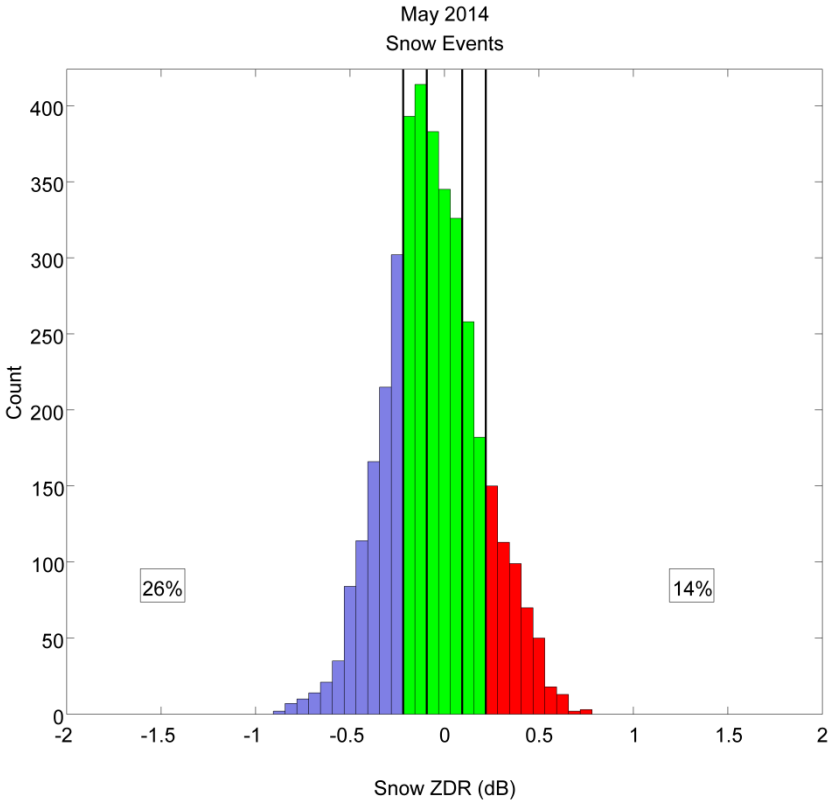

Figure 11b. Same as Figure 11a but for May 2014.

.

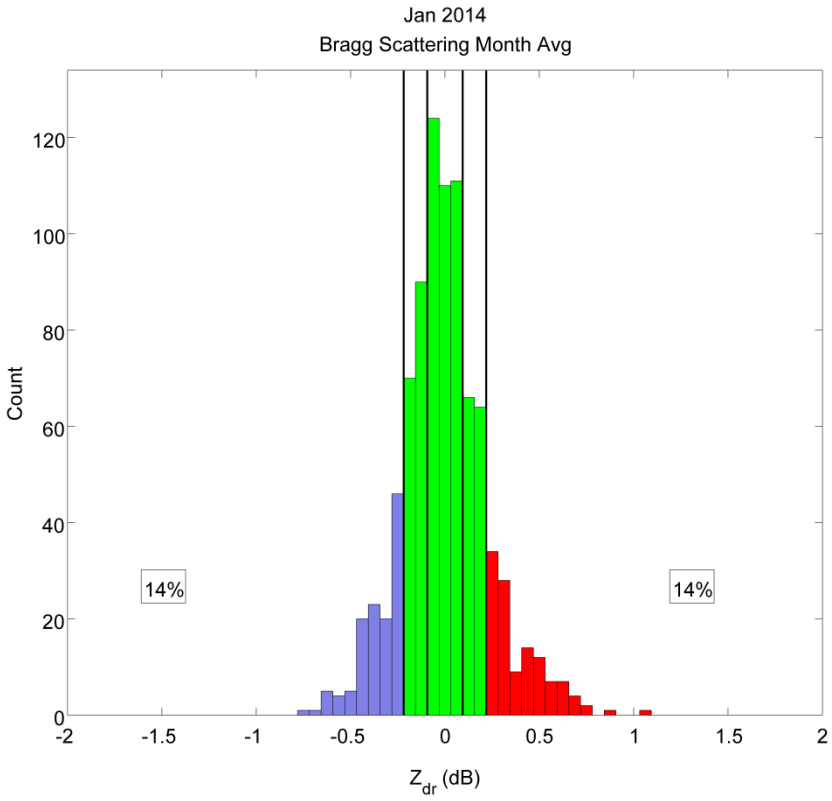

Figure 12a. Frequency distribution of median system Z_{DR} biases for the Bragg scatter method for January 2014.

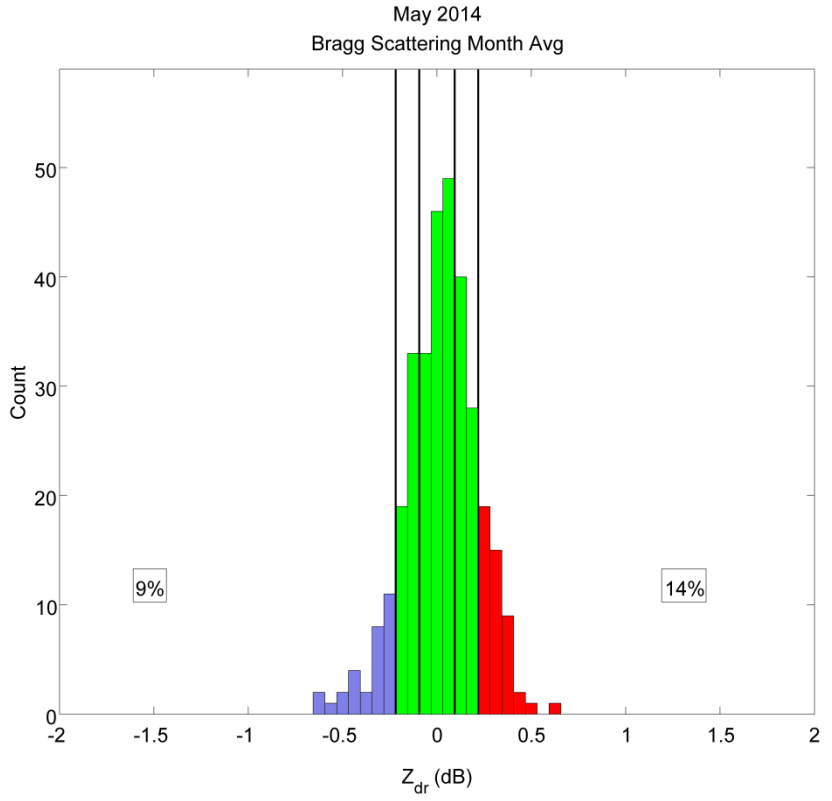

Figure 12b. Same as Figure 12a but for May 2014.

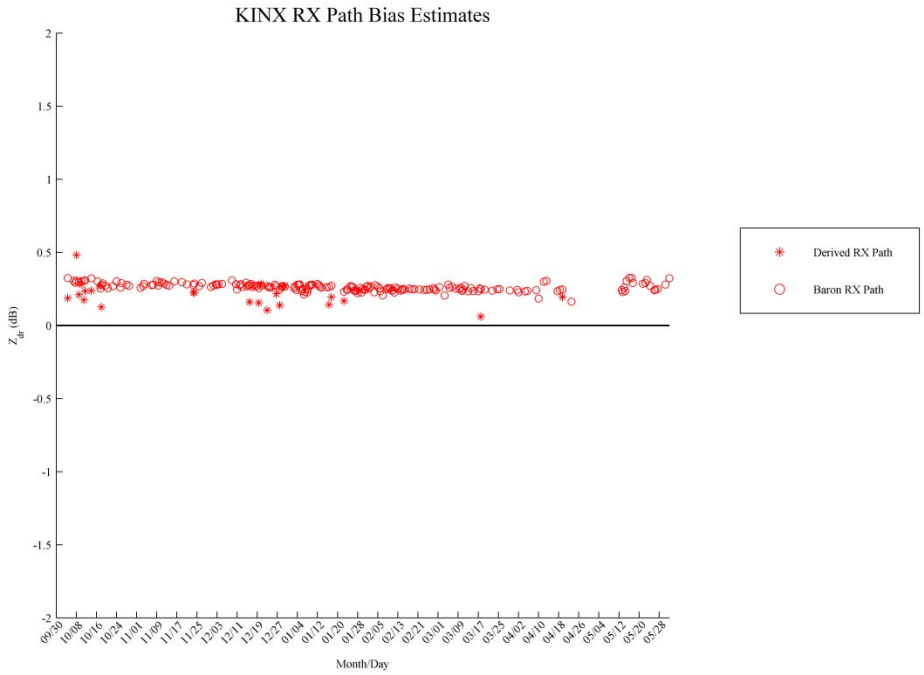

Figure 13a. Time series plot of receiver path bias estimates from sun spikes (Derived RX Path) and from the hardware receiver measurements (Baron RX Path) for the Tulsa, Oklahoma WSR-88D (KINX). The period of time starts the first of October 2013 and runs through end of May 2014.

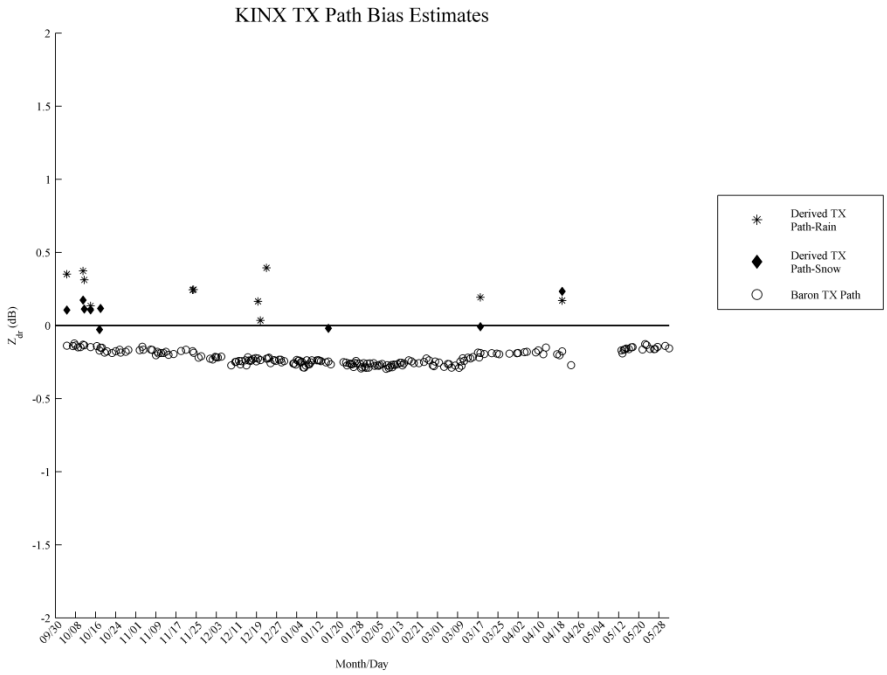

Figure 13b. Time series plot of transmitter path bias estimates estimated from light rain and dry snow (Derived TX Path-Rain, Snow) in combination with the sun spike receiver path bias and the hardware transmitter measurements (Baron TX Path) for the same time period as Figure 13a.